THE EFFECT OF DISTURBANCES ON A WING

RICHARD EPPLER
UNIVERSITAT STUTTGART
STUTTGART, WEST GERMANY

SUMMARY

Disturbances such as flap and aileron hinges and poorly faired spoilers were simulated in a computer wind tunnel. The total drag of a single roughness element does not depend only on the size of that element. Its position on the wing has a surprisingly strong effect. In particular, a roughness element on the convex side of a deflected flap or aileron causes a very substantial increase in drag. Very few experimental data are available for comparison. Good agreement with experiment can be achieved, however, by adapting a fictive "step size." The correlation between the real roughness-element size and the drag increase remains to be determined. Simple, fundamental experiments are suggested which will allow a theoretical estimation of the drag increase due to roughness elements.

INTRODUCTION

Disturbances on a wing due to flap and aileron hinges, variable chord arrangements, poorly faired spoilers, etc. become more significant as airplanes become more efficient. In other words, as the profile drag decreases, so must the parasitic drag. Performance differences between airplanes of the same type and performance differences between similar types have been measured several times. These differences indicate that some airplanes have parasitic drag due to seemingly insignificant details. It is necessary to investigate such details in the sense of Bruce Carmichael's study "What Price Performance?" (ref. 1). As long as we spend lots of money on variable chord concepts, we should at least be sure to take every opportunity to realize less expensive performance improvements. One such improvement could be the reduction of disturbances connected with flap and aileron hinges and with spoiler gaps and steps. These two-dimensional disturbances usually occur at wing positions where the boundary layer is already turbulent. Because there is very little experimental information on such disturbances, a theoretical disturbance model has been developed. It yields relative effects and indicates which simple, fundamental experiments are necessary to obtain a method for the estimation of the absolute amount of these effects.

THE DISTURBANCE MODEL

The boundary-layer flow in the region surrounding a two-dimensional disturbance of height h perpendicular to the wall is shown in figure 1. The velocity $u(y)$ in the boundary layer at $y = h$ is called u_h. It is plausible that the influence of the disturbance will depend mainly on h and u_h. This influence will be evident several step heights downstream (fig. 1). As long as h is not too large, the velocity $u(y)$ depends only on the wall shear stress τ_o. This was shown by Ludwieg and Tillman (ref. 2) and reconfirmed by Kader and Yaglom (ref. 3). A good approximation for $u(y)$ is

$$\frac{u(y)}{u_\tau} = a \log \frac{y u_\tau}{\nu} + b \tag{1}$$

where ν is the kinematic viscosity, $u_\tau = \sqrt{\frac{\tau_o}{\rho}}$ is the wall shear-stress velocity, and ρ is the density; a ($\approx$5) and b ($\approx$6.5) are constants. For use in a boundary-layer computation method, it is better to transform equation (1) by means of the local skin-friction coefficient $C_f = \frac{\tau_o}{\rho U^2}$ into

$$\frac{u(y)}{U} = \sqrt{C_f}\left[2.17 \ln \left(\sqrt{C_f}\,\frac{U}{U_\infty} R \frac{y}{L}\right) + 6.5\right] \tag{2}$$

where U is the local potential-flow velocity, $R = \frac{U_\infty L}{\nu}$ is the overall Reynolds number of the flow, U_∞ is the free-stream flow velocity, and L is the reference length which, for a wing, is the chord length c.

As long as this approximation is valid for u_h, the influence of the disturbance will depend only on the local disturbance Reynolds number

$$R_h = \frac{u_h h}{\nu}$$

It is even plausible that the displacement thickness δ_1 will change linearly with R_h. This means that the distance between the undisturbed and disturbed velocity distributions is proportional to $u_h h$. The same is approximately true for the momentum thickness δ_2 and the energy thickness δ_3. Therefore, the model to be used assumes that δ_2 is increased by a value.

$$\Delta\delta_2 = ku_h h \tag{3}$$

as a result of a disturbance of height h. It can be shown that the additional assumption

$$\Delta\delta_3 = \Delta\delta_2 \tag{4}$$

is also reasonable provided u_h is not too large. The most difficult problem is determining the value of the proportionality constant k. The value of this constant will depend on the precise shape of the disturbance. It should not be too difficult to obtain accurate values for k from simple experiments. Such experiments have been planned by F. X. Wortmann and D. Althaus of the Institut für Aerodynamik und Gasdynamik at the Universität Stuttgart.

If the boundary layer is laminar at the position of the roughness element, the computation predicts transition at that position.

DISTURBANCES ON A WING

A value of $k = 0.15$ was used in equation (3) as a rough approximation for a simple roughness element like a trip wire. A computer program was used to evaluate the effects of disturbances on a wing. Given the airfoil shape, the program computes the velocity distributions corresponding to the various input angles of attack. For all velocity distributions, boundary-layer computations are performed for the different input Reynolds numbers. Disturbances can be specified at up to two different positions on each surface of the airfoil.

Several examples illustrate the capabilities of this disturbance model. For the first example, one disturbance of height $h = 1$ mm was introduced at various positions along the upper surface of airfoil E603. The velocity distributions for various lift coefficients c_l are shown in figure 2. The roughness element was introduced at three different chordwise positions; $x/c = 0.4$, $x/c = 0.6$, and $x/c = 0.81$. The theoretical polars at $R = 1 \times 10^6$, which corresponds roughly to low-speed flight in a sailplane, and $R = 3 \times 10^6$, which corresponds to high-speed flight in a sailplane, are presented in figure 3. The results clearly indicate that the potential-flow velocity at the position of the roughness element has a strong influence on the drag. The additional drag nearly always increases with lift coefficient as does the local velocity. The polar for the most forward disturbance, however, has a different character. At $c_l \approx 1.1$, the most upstream roughness element has less influence than the more downstream ones. By looking into the details, it was determined that not only the potential-flow velocity, but also the skin-friction coefficient at the position of the roughness element has a strong influence.

If transition occurs in an adverse pressure gradient and the roughness element is shortly behind this transition, the turbulent boundary layer will not be fully developed at the position of the roughness element and the effect on the drag will, therefore, be quite small. Of course, the effect on the drag will be quite large if the roughness element shifts the transition point toward the leading edge.

These results are entirely theoretical. It is, of course, desirable to obtain a correlation between theory and experiment. It would be easy to perform wind-tunnel experiments which correspond to this example. As previously mentioned, these experiments are planned but have not yet been performed.

Experimental data applicable to this problem are rare. There have been many experiments concerning the influence of roughness elements on transition, but few on the effects of roughness elements on a boundary layer which is already turbulent. One such experiment was performed in 1971 by D. Althaus in a low-turbulence wind tunnel at the Universität Stuttgart. In that test, the polars of an airfoil (FX 62-K-153/20) with a conventional, center-hinged flap (gap sealed) were measured first. Then, the polars were determined for the same airfoil with a so-called "Elastic Flap" (ref. 4). These experiments are valuable for evaluating the theory because the two models differed only by the radius of the arc between the forward portion of the airfoil and the flap and by the single step (roughness element) which is a part of every flap hinged in the conventional manner.

The envelopes of the polars for both configurations are shown in figure 4. Each envelope was obtained by plotting the lowest drag coefficients for the various flap deflections at a given lift coefficient. This means that the drag coefficients for zero or negative (up) flap deflections are used for low lift coefficients and the drag coefficients for positive (down) flap deflections are used for high lift coefficients. Thus, the envelope is defined by the data for the optimal flap deflections. The differences between the two curves is quite small for the lower lift coefficients and surprisingly large for the higher lift coefficients.

For some time, no explanation could be found for this apparent anomaly. After introducing the disturbance model into the computer program, however, it was not difficult to analyze these two configurations theoretically. The velocity distributions for the FX 62-K-153/20 airfoil (ref. 5) using the original coordinates are shown in figure 5. Not unlike many Wortmann airfoils, the coordinates are not smoooth. The velocity distributions show irregularities, the worst one occurring at the leading edge on the lower surface. In the practical use of this airfoil and for the wind-tunnel model, these irregularities have probably been smoothed out. Therefore, it was reasonable to smooth the coordinates before

proceeding with further computations. The boundary-layer method is very sensitive to such irregularities, especially with regard to the prediction of transition. The velocity distributions for the smoothed airfoil with 0° and 10° flap deflection are shown in figure 6. The differences between the two flap configurations (plain and elastic) are evident only on the upper surface in the region around the hinge. The elastic flap causes a much lower suction peak at the hinge than the normal, plain flap. Moreover, the plain flap introduces a certain, single roughness element at that point. It was not possible to specify the height h of the roughness element in the disturbance model directly from the step height at the hinge. Instead, several different values for h were tried. The theoretical results for $h = 0.6$ mm at $R = 1 \times 10^6$ and 3×10^6 are shown in figure 7. Interestingly, the theory shows exactly the same phenomenon as the experiment. At 0° flap deflection, the differences between the two flap configurations are small, and at 10° deflection, the same roughness element causes a considerable drag penalty for the plain flap. For positive flap deflection, the roughness element is located precisely at the position of the suction peak, which means that it is in a region of high potential-flow velocity. Also, the increased favorable pressure gradient for the plain-flap configuration ahead of the element causes an increase in wall shear stress which further amplifies the drag penalty. For 0° flap deflection, the potential-flow velocity and the wall shear stress are much lower at the position of the roughness element, which explains the small difference for this case.

Some of the experimental data from figure 4 are included in figure 7. The drag penalties predicted by the theory agree well with the experiment. It must be emphasized that the absolute value of the drag penalty is not the significant result. This value was achieved by selecting the right value for h. The ratio between the drag differences with and without flap deflection, however, must be pointed out as a fundamental result which agrees well with experiment. This result, of course, has practical applications and can eventually explain some of the performance differences between similar airplanes. The order of magnitude of these drag differences should not be neglected in performance calculations.

The maximum lift coefficient and its decrease due to the roughness element were not predicted as well as the drag penalty. It should be noted, however, that the wind-tunnel results for maximum lift coefficient must be suspect. The wind tunnel used has a closed, rectangular test section with the model spanning the tunnel from wall to wall. The lift coefficient is determined by measuring the pressures along the top and bottom tunnel walls. Thus, these measurements yield the average c_l over the span of the model. Note also that the span is roughly equal to the chord. Accordingly, any separation at the juncture of the tunnel wall and the model influences the measured lift coefficient considerably.

CONCLUSIONS

Single roughness elements have been theoretically modeled. The data from a previously run experiment on a flapped airfoil with and without a disturbance at the hinge was used for comparison. The drag penalty predicted by the theory and measured in the experiment was large enough to account for performance differences between similar airplanes. It must be concluded, therefore, that more effort should be spent on dealing with this phenomenon. Some simple experiments should be performed to support the theory. More attention should be paid to the roughness elements on airplanes which originate near spoilers and near flap and aileron hinges.

REFERENCES

1. Carmichael, B. H.: What Price Performance? Soaring, vol. 18, no. 3, May - June 1954, pp. 6-10.

2. Ludwieg, H.; and Tillman, W.: Investigations of the Wall-Shearing Stress in Turbulent Boundary Layers. Ing.-Arch., vol. 17, no. 4, 1949, pp. 288-299.

3. Kader, B. A.; and Yaglom, A. M.: Similarity Treatment of Moving-Equilibrium Turbulent Boundary Layers in Adverse Pressure Gradients. J. Fluid Mech., vol. 89, part 2, Nov. 28, 1978, pp. 305-342.

4. Althaus, D.; and Eppler, R.: Airfoils With a New Hinge for Ailerons and Flaps. Motorless Flight Research, 1972. NASA CR-2315, 1973, pp. 205-217.

5. Althaus, D.: MeBergebnisse aus dem Laminarwindkanal des Instituts für Aerodynamik und Gasdynamik der Universität Stuttgart. Stuttgarter Profilkatalog I, Institut für Aerodynamik und Gasdynamik der Universität Stuttgart, 1972.

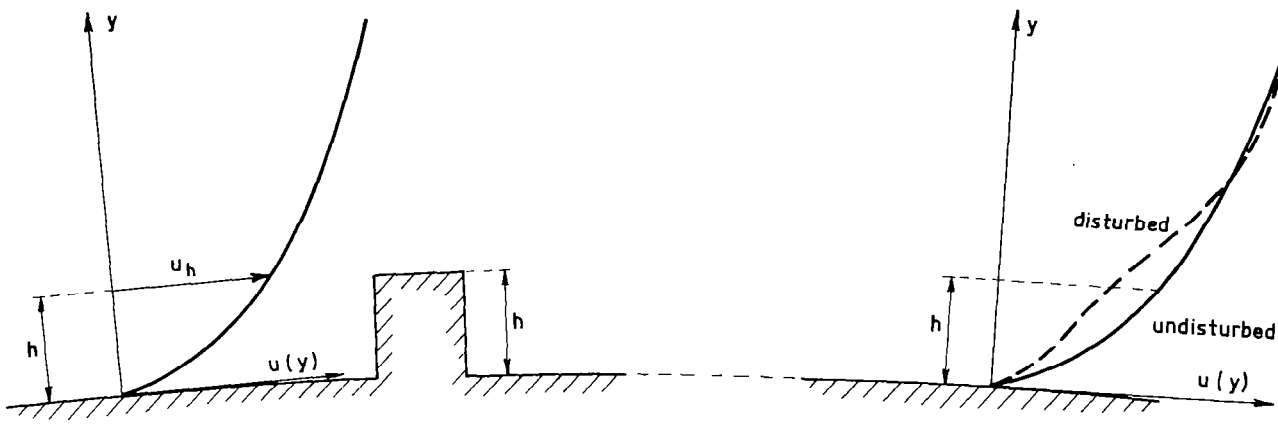

Figure 1.- Influence of disturbance on flow in boundary layer.

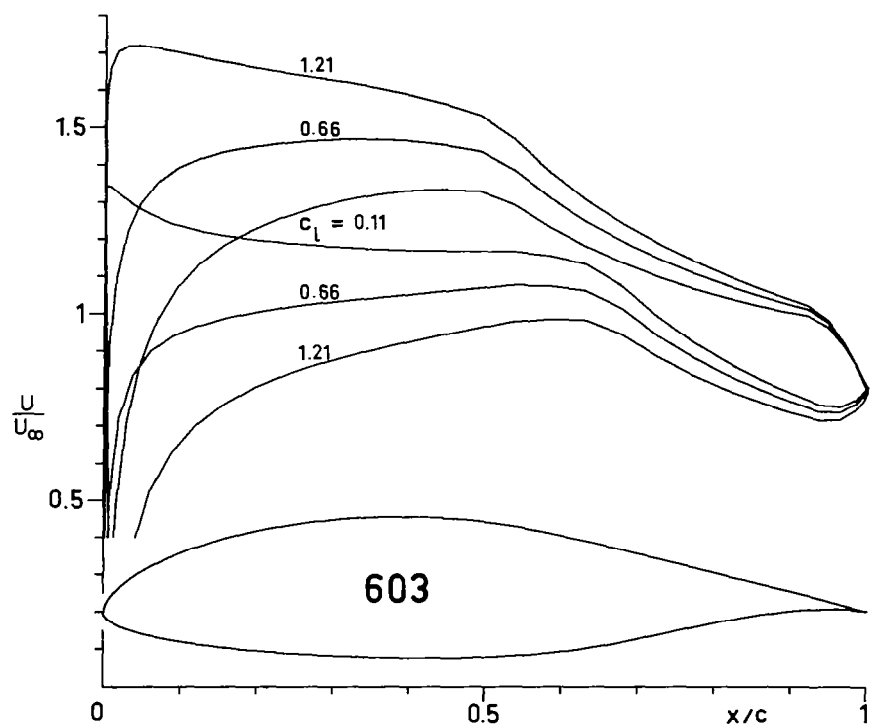

Figure 2.- Velocity distributions of airfoil E603.

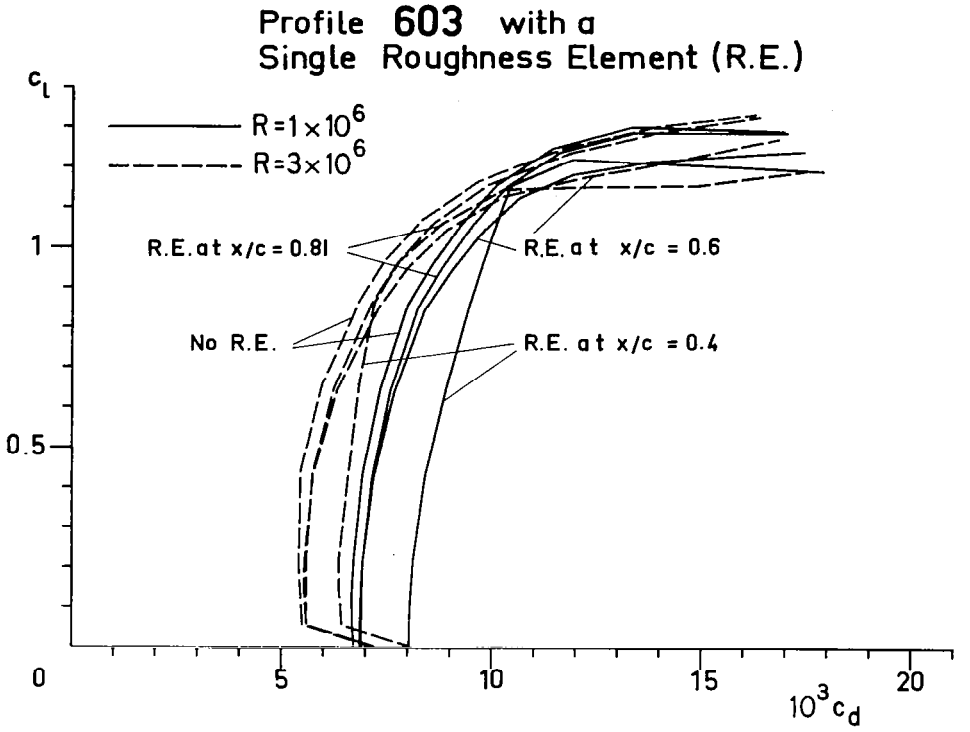

Figure 3.- Theoretical polars for airfoil E603.

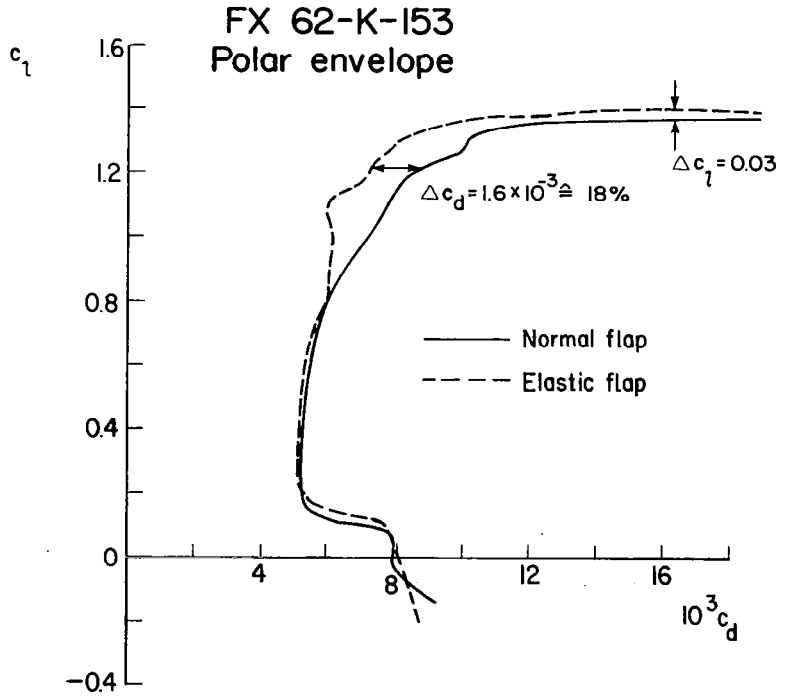

Figure 4.- Experimental envelope for FX 62-K-153/20 airfoil.

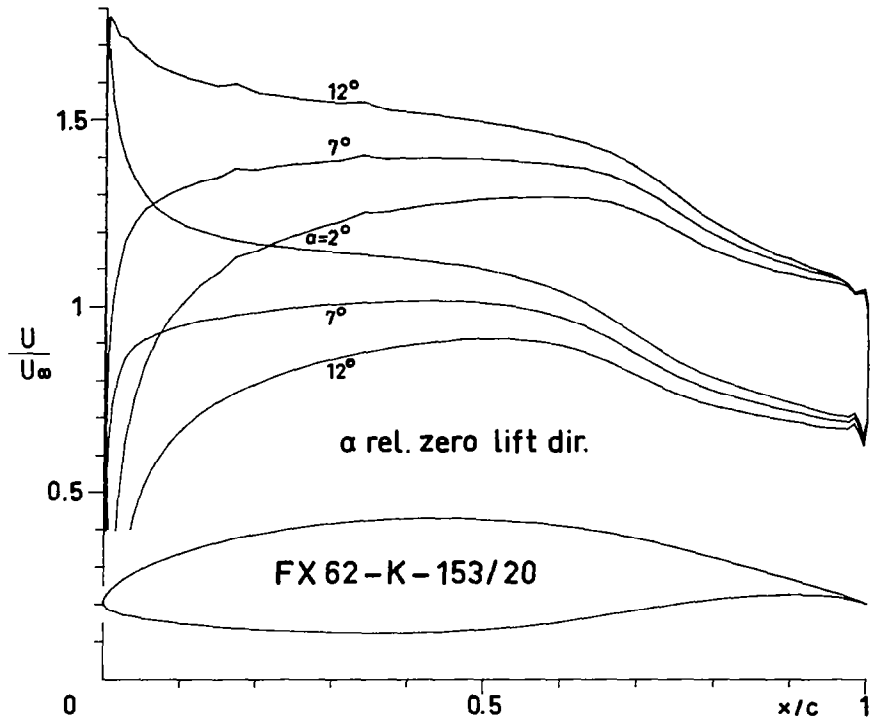

Figure 5.- Velocity distributions for FX 62-K-153/20 airfoil; original coordinates.

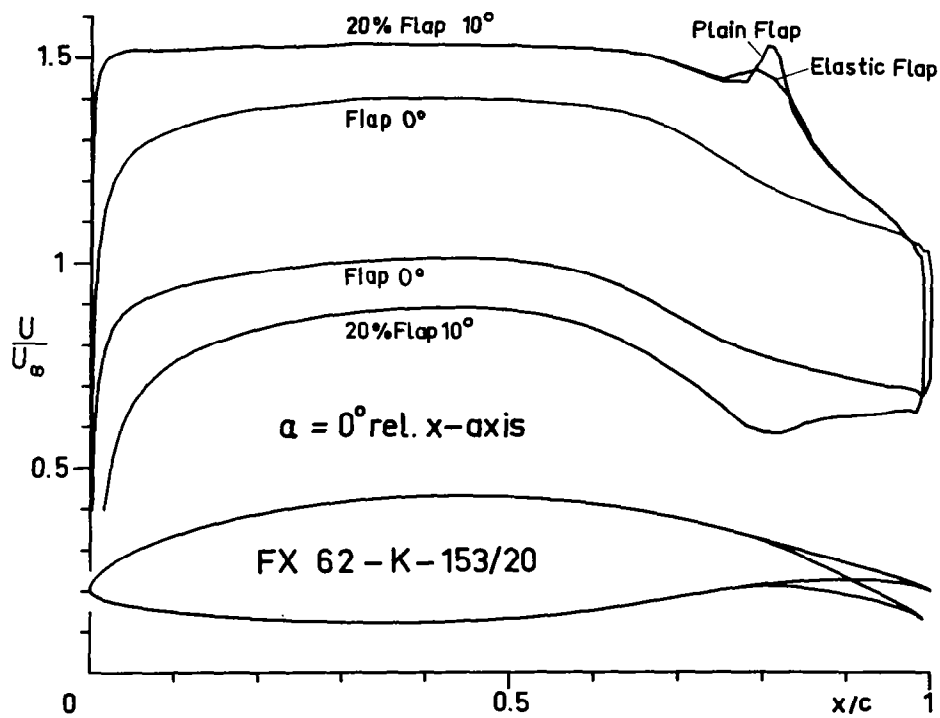

Figure 6.- Velocity distributions for FX 62-K-153/20 airfoil; smoothed coordinates.

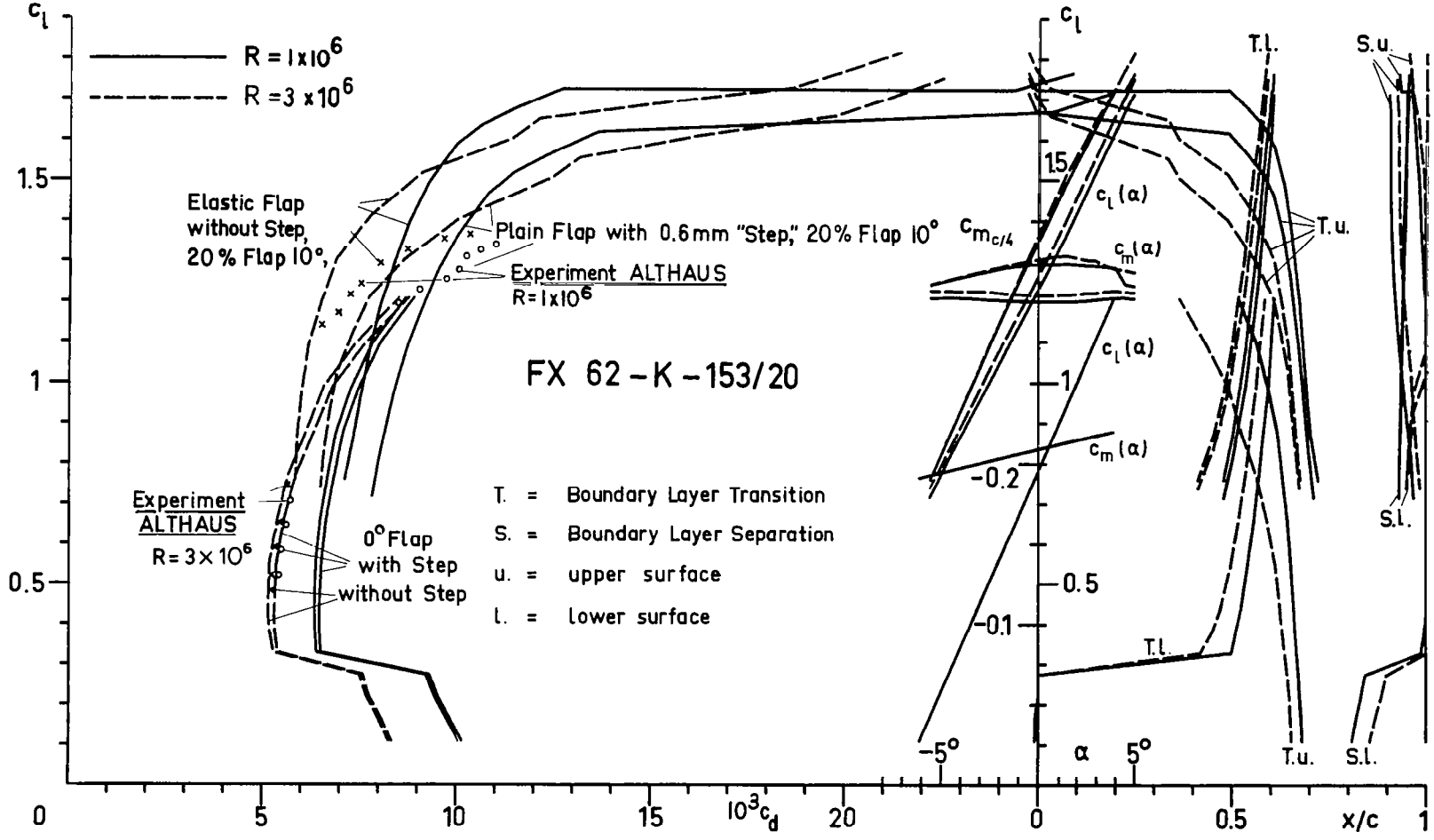

Figure 7.- Theoretical and experimental polars for FX 62-K-153/20 airfoil.